MEASUREMENTS AND NUMERICAL PREDICTIONS OF LIQUID AGENT DISPERSAL AROUND SOLID OBSTACLES*

Cary Presser and John F. Widmann
National lnstitute of Standards & Technology

Paul E. DesJardin and Louis A. Gritzo
Sandia National Laboratories

ABSTRACT

The focus of this effort is to investigate the dispersal of liquid agents around solid obstacles and to obtain a better understanding of the physical processes of droplet transport in cluttered spaces. A combined experimental/numerical study is presented to examine the flow field dynamics of highly turbulent flow over obstacles, and spray transport in such flow fields. Comparison of numerical predictions to the particle imaging velocimetry (PIV) measurements shows good qualitative agreement in spatial distribution of the mean and **RMS** velocities with a 20% overprediction in mean streamwise velocity and 15% underprediction in **RMS.** A numerical sensitivity study using HFE-7100 agent reveals a strong dependency of droplet penetration on initial droplet size for the flow range and droplet sizes of interest in practical agent delivery systems.

INTRODUCTION

The new generation of halon replacements includes chemical suppressants that have high boiling point temperatures (i.e., $T_b > 330$ K) and exist in liquid phase under high pressure release or in ambient conditions. Release of these agents in a confined space results in the dispersal of droplets that will either travel along ballistic trajectories, move with the convecting flow, or a combination of the two depending on the local Stokes number of the droplet. Therefore, accurate representation of droplet transport is crucial for numerical modeling of fire suppression in confined spaces using these agents. To better understand the physics of droplet dispersion around solid objects, an experimental arrangement at the NIST spray facility has been modified to impose controlled grid-generated turbulence on the air stream. Experimental results from this facility will provide new experimental data for a well-characterized, homogenous droplet-laden turbulent flow field around a prescribed obstacle. Baseline measurements of the single gas-phase velocities with and without obstacles, but without the spray, are reported in this study. Operating conditions are based on typical engine nacelle-like conditions, to study the atomization and dispersion of a liquid agent around three cylinders chosen as representative obstacles. The sizes of the tubes were chosen such that the diameters were smaller, similar to, and larger than the characteristic length scale of turbulence to explore turbulence generation or reduction due to clutter. In addition to the experiments, numerical simulations using the WLCAN Computational Fluid Dynamics (CFD) fire physics code are conducted and compared to the experimental measurements of gas mean velocity and turbulent kinetic energy. A sensitivity study is also conducted as part of the CFD calculations to explore the dispersal of liquid droplets around the obstacles as a function of initial droplet size. The motivation of this exercise is to understand the droplet transport processes that govern agent transport to regions behind solid objects.

This paper presents a description of the experimental arrangement, diagnostics used to characterize the flow field, and the CFD model. The results from both the experimental measurements and numerical simulations are compared and discussed, along with comments on future work.

EXPERIMENTAL ARRANGEMENT

To explore droplet transport around obstacles, an experimental arrangement is used that provides a well-characterized, homogeneous turbulent flow field around prescribed obstacles (Figures 1 and 2). The experimental facility includes an air swirl burner used in the reported experiments to provide nonswirling air to the experiment and coflows around the liquid agent injector.

* The numerical work was performed in part at Sandia National Laboratories, a multiprogram laboratory operated by Sandia Corporation, a Lockheed-Martin Co., for US Department of Energy, contract DE-AC04-94AL85000.

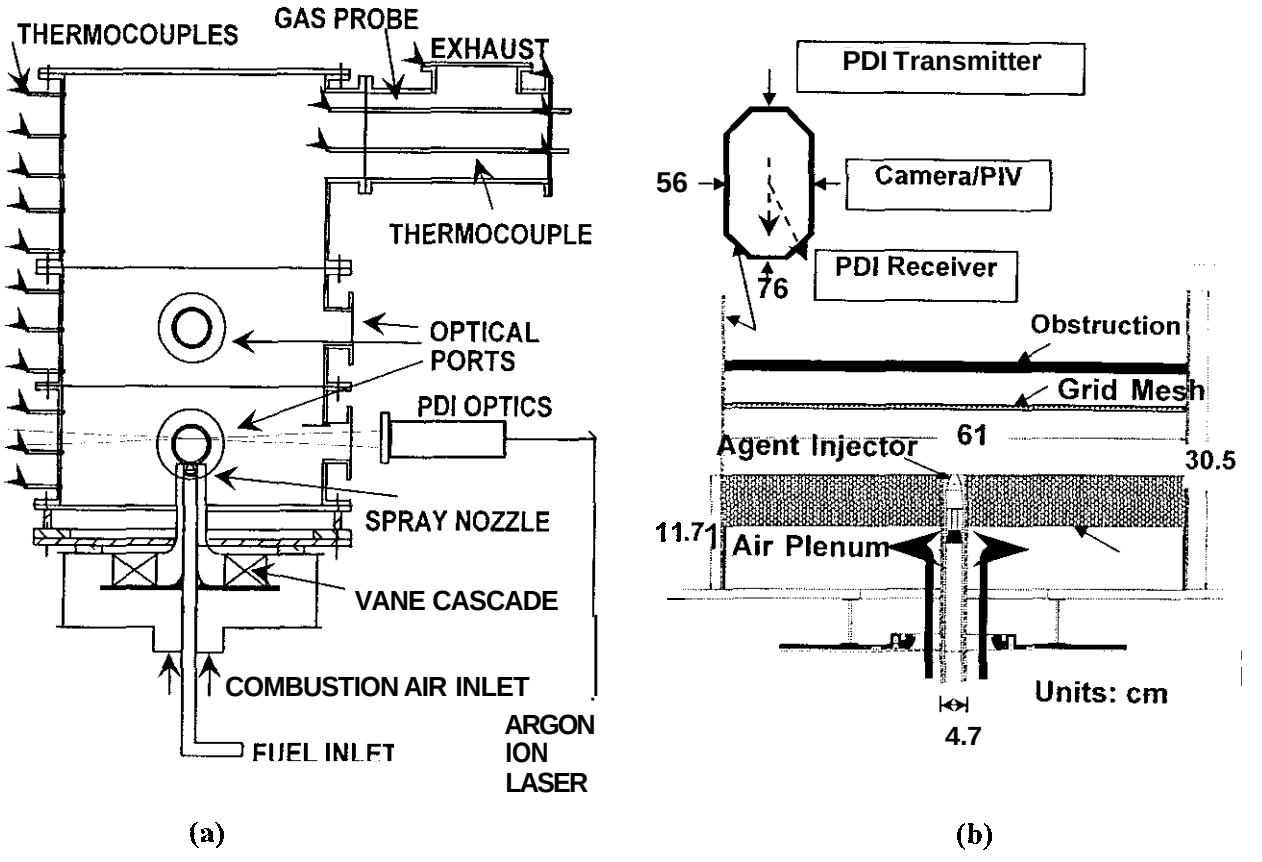

Figure 1. Schematic of (a) the reference spray facility, and (b) the general facility modifications for mesh-generated air turbulence.

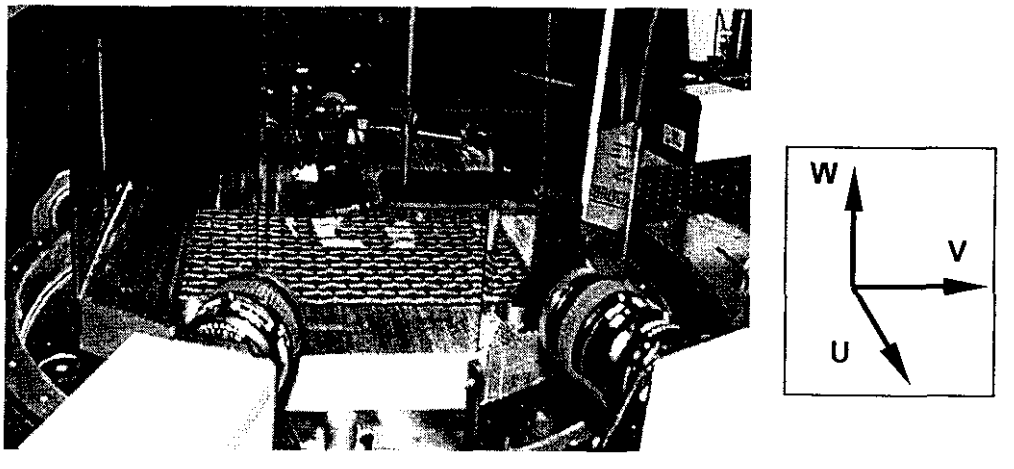

Figure **2.** View of the current experimental arrangement with cameras from the PIV system in the foreground.

Additional details on the design of the burner are available elsewhere [I]. Figure 1a shows the presence of a stainless steel enclosure to provide improved reproducibility and control of the spray and surrounding airflow field. The chamber height is 1.2 m, the inner diameter is **0.8** m, and several windows provide optical access. However, since the current experiments focussed on the gas stream turbulence, only the chamber base was used without the enclosure. (The enclosure will be used in the next phase of this work

in which liquid agent will be introduced to the turbulent flow field.) In place of the stainless steel enclosure, an octagonal Plexiglas insert (with a wall thickness of 6 mm) was used as a boundary condition (generically shown in Figure 1b). A honeycomb layer (51 mm thick with 3 mm size cells) is used to straighten the airflow, which is co-positioned around an injector for the agent. Grid-generated turbulence on the air stream is imposed by placing a layer of wire mesh screen (with 13 mm size cells) downstream of the honeycomb. For these experiments, the incoming air was directed entirely through a selected 125 by 254 cm rectangular cross sectional portion of the honeycomb and then through wire mesh screen (placed 25 mm downstream of the honeycomb) (Figure 2). The integral and Kolmogorov length scales of turbulence are estimated to be 3 cm and 100 pm, respectively. Three obstacle tubes (diameters of 3, 13, and 32 mm) were chosen to span ranges of clutter sizes smaller, on the same order, and larger than the integral length scales of turbulence. The obstacles were placed 100 mm downstream of the honeycomb. Choice of location of the screen and obstacles is discussed further in the next section. A stepper-motor-driven traversing system translates the entire assembly, and permits measurements of the flow field properties at selected locations downstream of the injector.

The mean gas velocities were initially estimated with a five-hole pitot probe and two-component phase Doppler interferometer. Although the overall results (as opposed to the detailed measurement profiles) are mentioned later in the text, a brief description of these two diagnostics is given here for completeness. The five-hole pitot probe has a hemispherical head that is 1.7 mm in diameter. The head is attached to a cylindrical body for a length of 26 mm, and then the diameter of the probe increases smoothly from 1.7 to 3.2 mm, which is the diameter of the main body of the probe. The probe has one hole on the head of the probe tip for total pressure measurements, and four holes located 13 mm from the head and 90 deg apart on the side of the probe for static pressure measurements. The average of the four velocity measurements is reported as the mean velocity. Mean gas velocities were also obtained at selected points by seeding the air flow field with 1 μm particles, generated with a pencil fogger, and using a two-component phase Doppler interferometer (PDI) from TSI, Inc.* This system will be used more extensively in the next phase of this work, in which liquid agent will be introduced to the flow field, to obtain spatial profiles of the droplet size and velocity distributions, and droplet number density. The receiving optics were aligned at a 25-deg scattering angle measured from the direction of propagation of the laser beams, and the transmitting and receiving optics were aligned at the same elevation. A 5 W argon ion laser operating in multiline mode was used as the illumination source. The blue (wavelength = 488 nm) and green (wavelength = 514.5 nm) lines of the argon ion laser are separated and focused by the transmitting optics to intersect and form the probe volume.

The flow field was characterized fully using a three-dimensional particle image velocimetry (PIV) system from Dantec Dynamics, Inc. PIV is a non-intrusive field measuring technique (as opposed to a single-point diagnostic method) that can measure two or three components of velocity. The method requires seed particles to be added to the flow, which are then assumed to follow the streamlines and act as tracers. The spatial displacement of the seed particles corresponding to two images separated by a known time period is measured, and the velocity is deduced. The seed particles generated by a pencil fogger were 1 μm in diameter. The images are obtained in a plane corresponding to the laser light sheet, and the time between the images is determined by the time between laser pulses. The spatial resolution of the measurements depends directly upon the pixel resolution, field of view, and laser light sheet thickness, and indirectly on the seeding density. For the measurements presented here, the spatial resolution is approximately 600 μm. The 3-D stereo PIV system differs from traditional PIV systems in that two CCD cameras are used, and three velocity components are measured [2].

* Certain commercial equipment or materials are identified in this publication to specify adequately the experimental procedure. Such identification does not imply recommendation or endorsement by NIST, nor does it imply that the materials or equipment are necessarily the best available for this purpose.

A 50 mJ Nd:YAG laser was used **as** the illumination source for the PIV measurements. The pulse duration of the laser light sheet was about 5 ns; the wavelength of the light was 532 nm. A pair of 12-bit double-frame CCD cameras with a resolution of 1024 x 1280 pixels was used to obtain the images. Special camera mounts were used to permit the rotation of the camera body with respect to the camera lens so that the Scheimpflug condition was satisfied, permitting the laser sheet to be in focus despite the non-orthogonal camera alignment [2]. Bandpass filters (center wavelength = 532 nm, acceptance window = 30 nm) were used to reject the broadband white light from the room. The two cameras were placed at angles of about 70 and 110 deg, as measured from the direction of propagation of the laser pulse. The processed results are presented **as** a composite mapping of individual planar regions that are about 40 mm in height and 50 mm in width. Statistics were obtained from about 500-700 individual records. Each field of view represents about 9000 vectors. Measurements of the flow field were carried out along the centerline of the measurement area, and at two planes, ± 25 mm from the centerline location.

CFD SPRAY MODELING

As a complement to the experimental measurements, a general-purpose fire simulation code, VULCAN, was used to conduct a parametric study of spray transport around the largest of the cylinders considered in the experiment. Specific details on numerical methods and modeling used in VULCAN, **as** well as the spray model, can be found in DesJardin et al. [3]. **A** 3D mesh was generated for the entire experimental facility with a total grid size of 26 x 51 x 80 = 106,080 cells. The initial conditions of the calculation are chosen to best match the experiment by setting the mean streamwise velocity, turbulence kinetic energy and its dissipation to values of 4.5 m/s, 0.304 m^2/s^2 and 0.0212 m^2/s^3, respectively. The agent considered in this parameter study is HFE-7100 ($C_4F_9OCH_3$) [4]. Many of the thermodynamic parameters of HFE-7100 needed for input to the spray model are available from the manufacturer and summarized in Table 1. However, the gas-phase enthalpy of HFE-7100 is not readily obtainable, and so only one-way coupling of the gas phase onto the spray transport is explored in this study. Future studies will consider two-way coupling effects.

TABLE 1. THERMODYNAMIC PARAMETERS OF HFE-7100

Property	Value
Molecular Weight	250 g/mol
Boiling Temperature	334 K
Critical Temperature	468.3 **K**
Heat of Vaporization @ B.P.	111.6 kJ/kg
Specific Heat @ room temperature	1183 J/kg
Density @ room temperature	1520 kg/m^3

RESULTS AND DISCUSSION

Preliminary characterization of the flow field uniformity was determined by means of planar Mie scattering flow visualization, pitot probe, and a two-component phase Doppler interferometer for different airflow speeds. The results indicated a flow mean velocity of 4.5 m/s, corresponding to a Reynolds number of 3700 (based on the grid cell size), provide a homogenous distribution of turbulence across the measurement area. This flow velocity is **also** representative of airflow speeds through aircraft engine nacelles.

Particle image velocimetry (PIV) was used to obtain instantaneous two-dimensional images of the airflow field velocity (i.e., three components of velocity). These images are then used to construct the streamwise (W) and two cross-stream (U and V) mean and root mean square (RMS) profiles, both upstream and downstream of the cylinder, and along the centerline location. Downstream of the honeycomb, the baseline flow field was found to be relatively uniform throughout the measurement field (Figures 3 and 4)

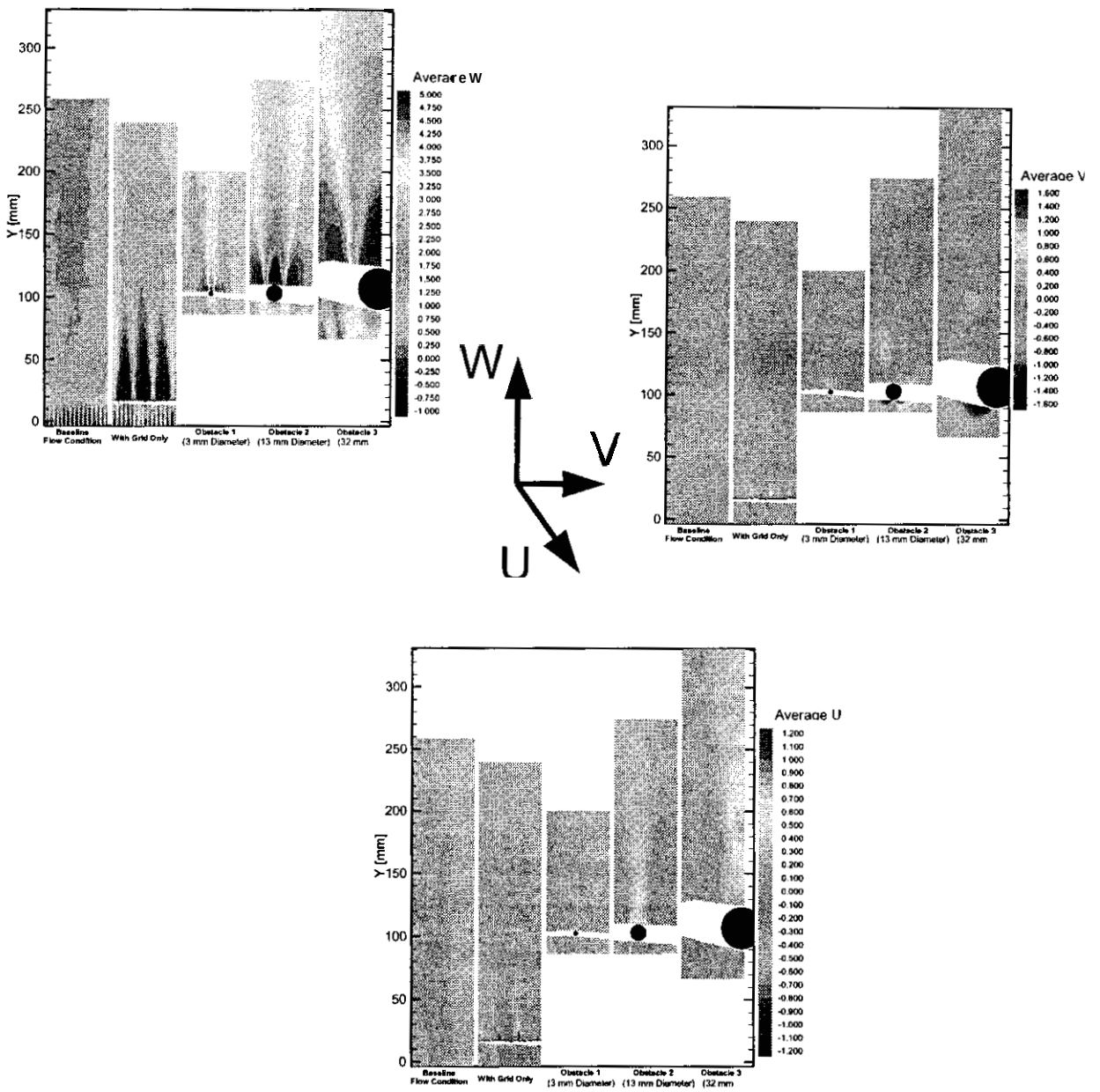

Figure 3. Variation of mean streamwise and cross-stream velocities with downstream distance.

(gas streamwise component of velocity, $v_W \cong 4.5$ m/s, and turbulence intensity, $\tau_W \cong 13\%$), except immediately downstream of the honeycomb. The local jetting downstream of the honeycomb exit decays with increasing streamwise distance and becomes negligible after 25 mm. Based on this observation, the wire grid mesh to generate turbulence is placed at this location. The flow downstream of the wire mesh was obtained along the centerline of the measurement region. Nonuniformities of the flow due to the mesh are created downstream of the mesh and relaxed to roughly a homogeneous state of 9% turbulence intensity in each direction at 100 mm downstream of the honeycomb ($v_W \cong 4.0$ m/s). The obstacles are placed at this location, shown with black circles, to study the effects of the turbulence and eventually spray transport around the cylinders in this well-controlled turbulent environment. The velocity accelerates to $v_W \cong 5.0$ m/s around the side of the cylinders and forms a recirculation region behind the cylinders ($v_W \cong -1.0$ m/s). The turbulence intensity increases behind the cylinder ($\tau_W \cong 20\%$ in a banded region behind the obstacle). The flow also decelerates to a stagnation region at the centerline, upstream face of the cylinders.

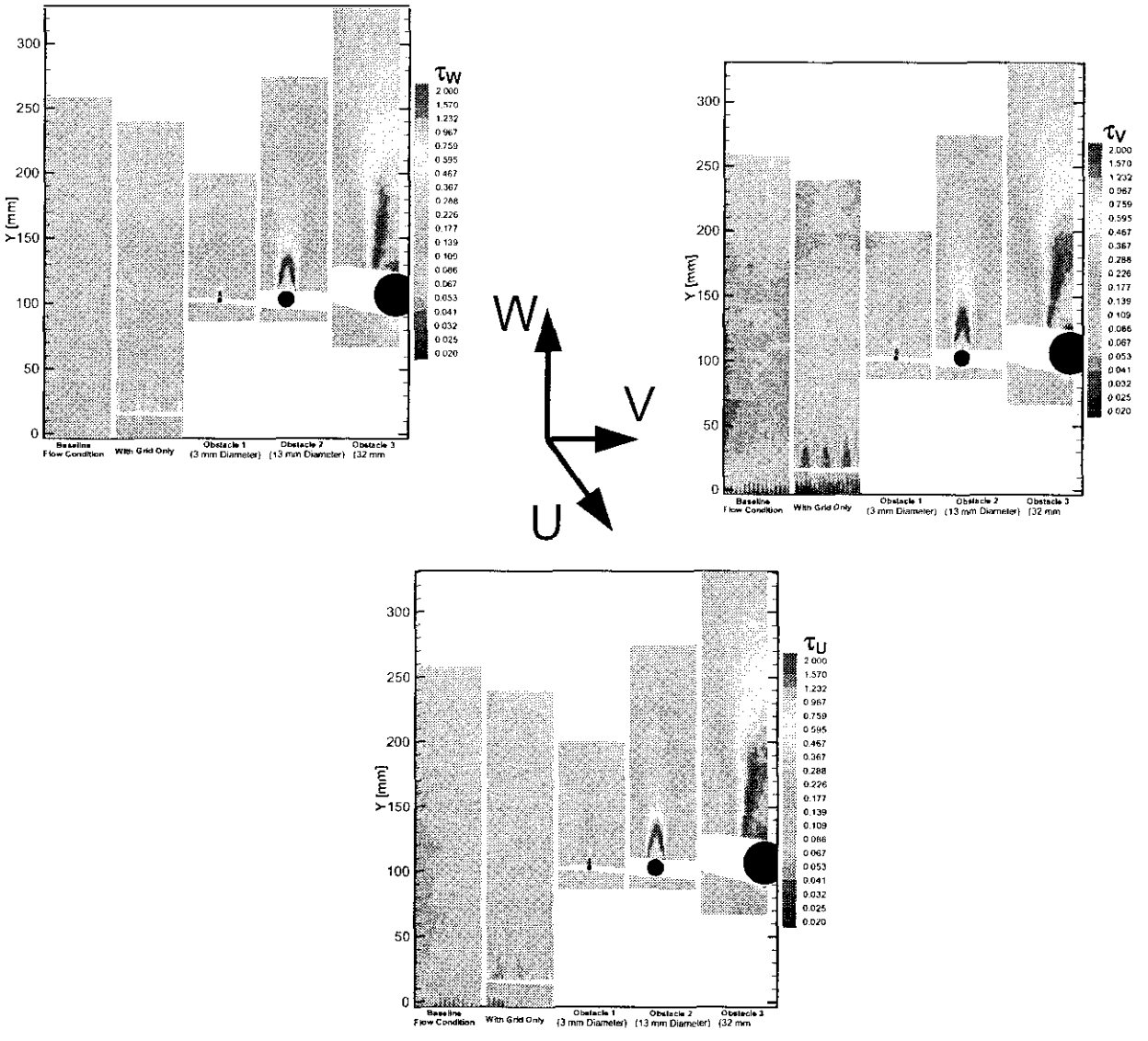

Figure 4. Variation of mean streamwise and cross-stream turbulence intensities with downstream distance.

Figures 3 and 4 indicate that for all three cylinders a strong recirculation zone is present on the downstream side of the cylinder with a large increase in turbulent kinetic energy. Comparisons of the CFD predictions (Figures 5 and 6) to the PIV measurements indicate that qualitatively the location and size of the recirculation zone for the largest cylinder case are well captured. A two-dimensional slice of the mesh (Figure 5a) shows local grid refinement in regions near the cylinder to resolve the shear layer properly. Quantitative comparison indicates that the numerical results overpredict the streamwise mean velocity by 20% and underpredict the RMS in strcamwise velocity by 15%. These differences indicate that the numerical predictions underestimate the extent of turbulent mixing behind the cylinder, which may be attributed to the use of the k-ε model, which is known *to* perform poorly in highly recirculating flows.

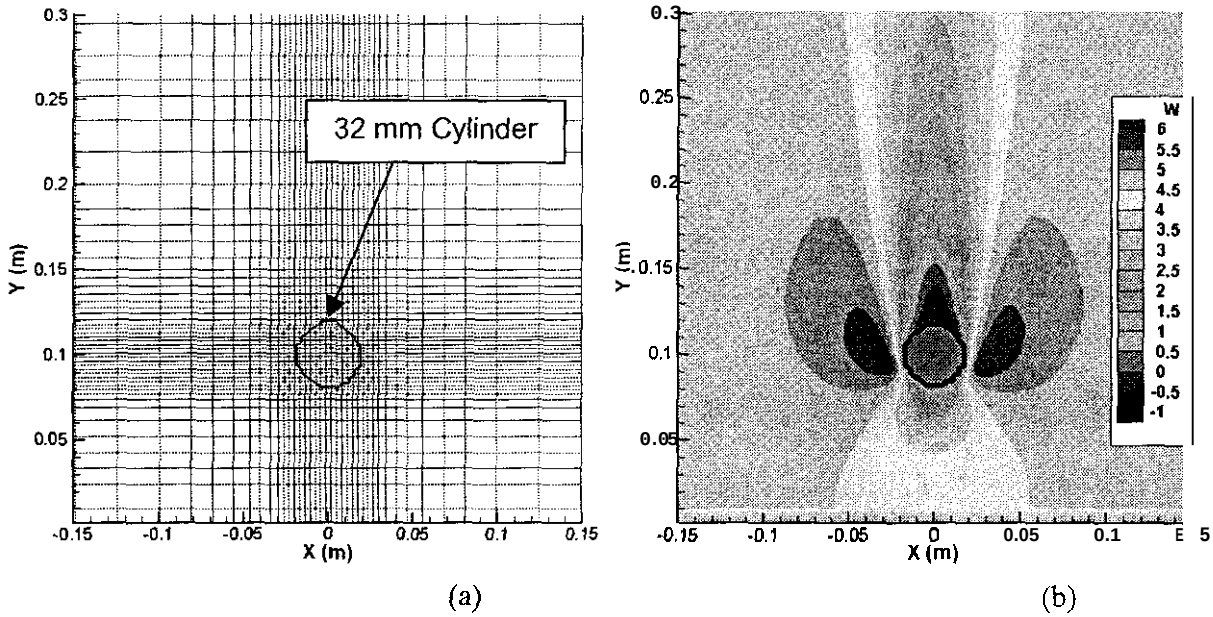

Figure 5. Cross-sectional views of CFD mesh showing (a) mesh refinement around the cylinder and (b) mean streamwise velocity.

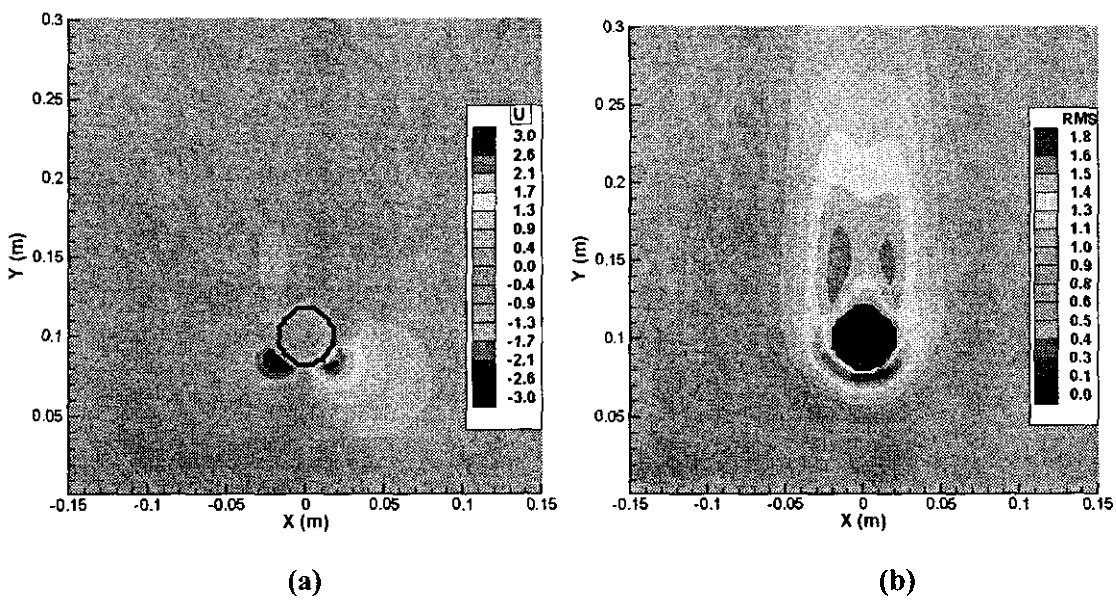

Figure *6:* CFD predictions of (a) mean cross-stream velocity and (b) estimate of cross-stream fluctuation.

The next experimental phase of this work is to inject a liquid fire suppressant agent and to study the change in droplet transport as the spray interacts with the obstacles. One possible choice is HFE-7100 (boiling point of **334 K)** since it has shown to be effective at extracting heat from a flame zone **[4].** Preliminary modeling results of this arrangement are shown in Figures 7 and 8. The spray is modeled as a stream of droplets with a mass load rate of 1.598 g/s and zero slip for the droplets (i.e., a droplet streamwise velocity of **4.5** m/s). Figures 7 and 8 present instantaneous snapshots of the spray distribution and velocity for three assumed droplet sizes of 10 pm, 50 μm, and 100 μm. These droplet sizes, chosen to span the range of credible scenarios during agent release, illustrate some interesting behavior. Figures 7a and 7b present results for the extreme 10 μm and 100 μm droplet cases. In both cases, the droplets are

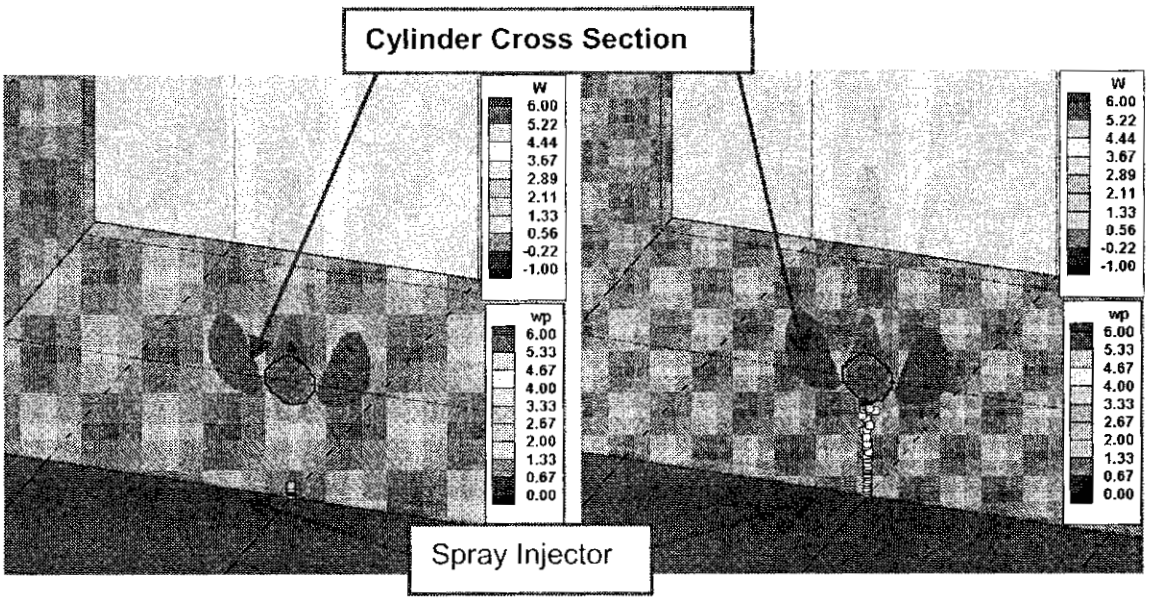

Figure 7. Instantaneous snapshots of spray impacting the 32 mm cylinder for (a) 10 μm, and 100 μm droplets

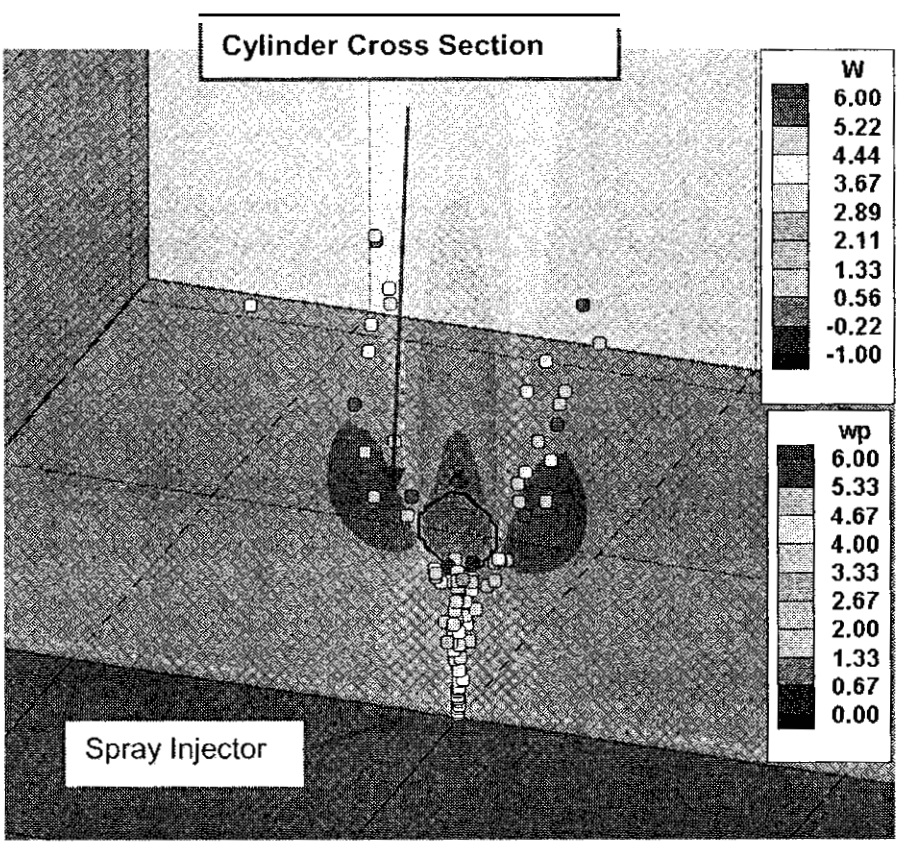

Figure 8. Instantaneous snapshot of spray impacting the 32 mm cylinder for 50 μm droplets

unable to penetrate beyond the cylinder because they are either too small and evaporate before reaching the cylinder (i.e., the 10 μm case) or too large and follow a ballistic trajectory that results in direct impact into the cylinder (i.e., the 100 μm case). However, the 50 μm case is able to penetrate beyond the cylinder (Figure **8).** In this case, the droplets are large enough not to evaporate too quickly, yet small enough to follow the streamlines and accelerate around the cylinder. Future efforts will focus on exploring this scenario experimentally, as well as investigating other realistic liquid agent release conditions.

CONCLUSIONS

PIV measurements and numerical predictions of a turbulent flow over cylindrical obstacles are presented. Comparisons of the flow field CFD predictions to the measurements show reasonable agreement. A numerical sensitivity study of initial droplet size reveals that droplet penetration around obstacles is dependent on droplet size. Future efforts of this work are to better understand these sensitivities for optimization of liquid suppressant delivery systems on larger scale experimental platforms.

ACKNOWLEDGMENTS

The authors wish to acknowledge the partial support of this work by the Department of Defense Next Generation Fire Suppression Technology Program, co-funded by the DoD Strategic Environmental Research Development Program. The authors also wish to thank Dr. G. Papadopoulos of Dantec Dynamics, Inc. for his assistance in recording and post processing the PIV results, and Mr. R. Fink for his assistance in completing the NIST facility modifications.

REFERENCES

1. Widmann, J.F., Charagundla, S.R., Presser, C., and Heckert, A., ***Benchmark Experimental Database for Multiphase Combustion Model Input and Validation: Baseline Case,*** Internal Report No. **6286,** National Institute of Standards and Technology, Gaithersburg, MD, 1999.
2. *Flowmap® 3D-PIV System Owner's Manual,* Dantec Measurement Technology, Inc., Mahwah, NJ, July 1999.
3. DesJardin, P.E., Gritzo, L.A., and Tieszen, S.R., "Modeling the Effect of Water Spray Suppression on Large-Scale Pool Fires," ***Proceedings,*** Halon Options Technical Working Conference, Albuquerque, NM, pp. **262-273,2000,**
4. Yang, J.C., Bryant, R.A., Huber, M.L., and Pitts, W.M., "Experimental Investigation of Extinguishment of Laminar Diffusion Flames by Thermal Agents," ***Proceedings,*** Halon Options Technical Working Conference, Albuquerque, NM, pp. **433-446,2000.**